A NOVEL POSE CONTROL METHOD OF 3-PRS PARALLEL ROBOT

Jianli Kang[1], Guoqiang Chen[1], Yahui Qiao[2], Fei Yang[3], Yuegong Wang[3]*
[1]School of Mechanical and Power Engineering, Henan Polytechnic University, Jiaozuo 454003, China
[2]School of Intelligent Engineering, Zhengzhou College of Finance and Economics, Zhengzhou, 450000, China
[3]Technology Center, Pingdingshan PMJ Coal Mine Machinery Equipment Co.,Ltd., Pingdingshan, 467100, China
*E-mail(s): *kangjl@hpu.edu.cn*(✉) (corresponding author's e-mail)

Abstract - Aiming at the pose variation of the fixed base in a wide range of applications, a novel pose control method for the 3-PRS parallel robot is proposed. The method uses the parallelism between the moving platform plane and the horizontal plane as the evaluation metric. The structure and equivalent model of the 3-PRS parallel robot are presented, and the coordinate systems of the robot and the local-level horizontal plane are established. The detailed expression of the angle of the moving platform plane and the horizontal plane and its derivation process are both presented. An implementation procedure is proposed for the proposed control method that is transformed into a constrained nonlinear optimization problem. To reduce the optimization complexity and improve computational efficiency, an optimization variable reduction strategy is proposed to transform the optimization problem with three variables into one with two variables. The genetic algorithm is used to solve the optimization problem in this study, and the key calculation process is given. The interval range of the optimization variables can be adjusted using a multi-stage method to find the global optimal solution while maintaining efficiency. The proposed method is validated in terms of its effectiveness, practicality, and feasibility using several typical application cases. The results show that the proposed method has many advantages and beneficial effects. The study provides a theoretical basis and timely support for the high-precision pose control of equipment on mobile platform, such as those used in intelligent production line, emergency rescue vehicle and intelligent driving.

Keywords: 3-PRS parallel robot, Pose control, Parallelism, Control method, Genetic algorithm, Optimization variable reduction, Multi-stage method.

1. Introduction

The 3-PRS parallel robot is a typical representation of a lower-mobility robot. The name of the 3-PRS robot is a vivid description of its structure. It consists of three identical kinematic chains, each containing three types of joints, connecting a fixed base platform and a moving platform. Each kinematic chain includes one prismatic joint (abbreviated as P), one revolute joint (abbreviated as R), and one spherical joint (abbreviated as S). The 3-PRS parallel robot has significant advantages such as simple structure and control, high stiffness and load capacity, fast dynamic response, high precision, compact structure with isotropy, and high task suitability [1,2]. It holds great application value in fields such as aerospace, intelligent manufacturing, emergency rescue, and intelligent transportation [3-8]. The 3-PRS parallel robot can be used as part of vehicle-mounted equipment to achieve precision and special application operations. The 3-PRS parallel robot can be installed on vehicles such as trucks, trailers, and emergency rescue vehicles, turning it into a mobile precision operation platform.

For example, after the 3-PRS parallel robot is combined with a vehicle-mounted platform, it has the following directions in the field of emergency management. In terms of emergency rescue and relief operations, the 3-PRS robot can be installed on vehicles such as trucks or special rescue vehicles, with its moving platform integrating tools such as grippers, breaking hammers, and cutting saws, forming a mobile precision operation platform. In terms of firefighting and reconnaissance, the vehicle-mounted 3-PRS robot can serve as a stabilization platform for actuators or as a pointer for reconnaissance equipment. In terms of medical aid and casualty transport, the platform motion is actively controlled to counteract the vehicle's pitch, roll, and heave. In terms of temporary on-site

dx.doi.org/10.17683/ijomam/issue24.19

processing and maintenance during emergencies, motorized spindles, welding torches, or 3D printing heads are integrated onto the moving platform.

In intelligent manufacturing, 3-PRS parallel robots excel in applications where precision, stiffness, and dynamic response are paramount [4, 9,10]. Their primary role is to act as a highly compliant and accurate end-effector or core module, tackling complex operations beyond the capability of conventional serial robots. In precision assembly, the 3-PRS configuration is designed as a lightweight, multi-degree-of-freedom force-controlled end-effector mounted at the end of an industrial robot arm. In the specialized precision material handling, it is applied to the transportation of large, fragile flat-panel materials, significantly enhancing both the stability and safety of the handling process. In hybrid industrial robotics, the 3-PRS parallel robot is often used as a basic module. Connected in series or parallel, it creates hybrid robots with more DOF for applications in material handling, robotic welding, and complex surface machining.

In the field of intelligent transportation, applications of the 3-PRS parallel robot are beginning to emerge. The 3-PRS parallel robot can be applied to battery swapping solutions for electric vehicles, as well as serve as a pan-tilt carrying a combination of multiple sensors [8].

The applications mentioned above all face a common problem: the position and pose of the fixed platform of the 3-PRS parallel robot dynamically changes. This involves theoretical modelling, performance optimization, intelligent control, and so on. Kinematic and dynamic analysis forms the foundation of research, aiming to establish precise mathematical models to describe and predict the motion and force conditions of the robot, including kinematic and dynamic modelling [11-16]. The 3-PRS robot is a multiple-input and multiple-output, strongly coupled, and nonlinear system, and advanced control algorithms are the key to achieving its excellent performance, including intelligent algorithm optimization control, trajectory planning and scheduling, and so on[17-20]. The evaluation and enhancement of key performance indicators such as stiffness, workspace and singularity, and actuating forces also constitute a focal point of research. Based on the 3-PRS configuration, research explores variants of the mechanism to expand application scenarios; through multi-objective optimization including kinematic transmission, workspace, stiffness and total mass, robots for specific tasks are developed [21-29].

A typical application of the 3-PRS parallel robot is in the low-altitude economy, serving as a UAV storage hangar for coordinated operations between vehicles and drones. Drone hangars can be either single-story or multi-story. Drone hangars can be either single-story or multi-story, meaning that a vehicle can carry one or more drones. The drone hangar is mounted on a vehicle platform. The vehicle travels with the hangar to a suitable location, achieving coordinated takeoffs and landings of multiple drones and efficient operation through intelligent scheduling. The drones that are launched carry out operational tasks, such as emergency surveying, while those staying behind in the hangar are recharging to replenish energy. The onboard generator or high-capacity batteries supply ample energy for recharging the drones. The pose of the platform plays an extremely important role in the safe takeoff, landing, and securing of the drones, thus making its levelness critically essential. Therefore, this study focuses on the vehicle-mounted drone hangar scenario, while also considering applications in other contexts, to research control methods for the 3-PRS parallel robot's motion platform.

The 3-PRS parallel robot features two rotational degrees of freedom and one translational degree of freedom [1, 2]. These two rotational degrees can be fully leveraged to dynamically compensate for pose changes of the fixed base and platform, while the translational degree is utilized to adjust for changes in height. Therefore, starting from the perspective of the moving platform being parallel to the horizontal plane, this study proposes a new concept of minimizing the angle between the two and develops novel control techniques. The core contributions of this study are as follows: a novel control approach has been proposed and solved using optimization methods, and its practicality, effectiveness, and feasibility have been validated through case studies.

This paper is structured as follows. Section 2 introduces the model of the 3-PRS parallel robot and establishes both the local local-level coordinate frame and the world coordinate frame. Section 3 proposes a novel control method and provides a detailed derivation process. Section 4 presents the specific implementation process. The proposed method is validated in terms of its effectiveness, practicality, and feasibility in Section 5. Finally, Section 6 summarizes the paper.

2. Structure of 3-PRS Parallel Robot with Real-time Dynamic Fixed Base

The schematic representation of the 3-PRS parallel robot is shown in Figure 1. The robot is composed of a moving platform, three limbs, three vertical rails and a fixed base. Three vertical rails are vertically linked to the fixed base B_1 B_2 B_3 . And B_1 B_2 B_3 form an equilateral triangle that lies on a circle of radius R . The axis of the revolute pair/joint R_i for $i = 1, 2$ and 3 is perpendicular to the prismatic pair/joint. Each limb L_i for $i = 1, 2$ and 3 with the length of l_i connects the corresponding rail by a prismatic pair R_i . The moving platform and three limbs are connected by three spherical

pairs/joints b_1, b_2 and b_3. Three spherical pairs form an equilateral triangle that lies on a circle of radius r. The feed of the prismatic pairs is given as H_i for $i=1,2$ and 3. The included angle θ_i for $i=1,2$ and 3 is defined from the vertical rail to its corresponding limb L_i.

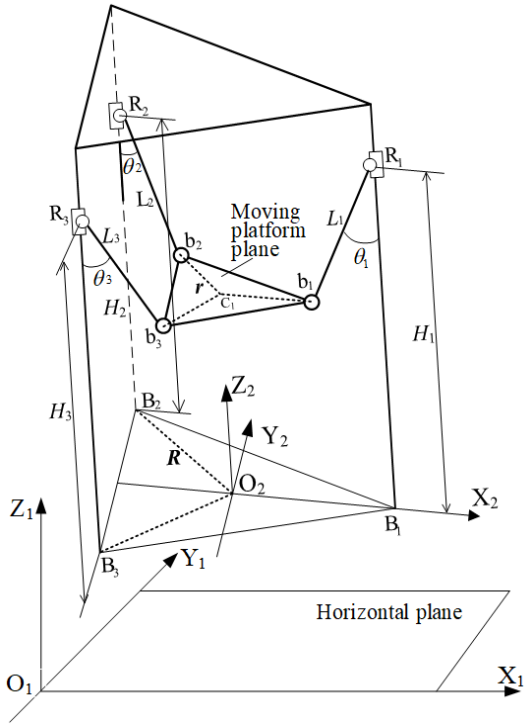

Figure 1: Schematic representation of the 3-PRS parallel robot with real-time dynamic fixed base

Two coordinate frames are used, as shown in Figure 1. One is the local-level coordinate frame $O_1X_1Y_1Z_1$ with the XOY plane corresponding to the local horizontal plane, the other coordinate frame $O_2X_2Y_2Z_2$ is located at the center O_2 of the fixed base $B_1B_2B_3$. X_2-axis and Y_2-axis are in the base plane $B_1B_2B_3$, X_2-axis points in the direction of O_2B_1, and Z_2-axis is normal to the fixed base plane and points upward. When the parallel robot is mounted on a mobile platform, the position and orientation of its fixed base changes in real time. Therefore, the position and pose of $O_2X_2Y_2Z_2$ can be described using the coordinates (x_T, y_T, z_T) of the coordinate origin and three Euler angles α, β and γ rotating about three axes of $O_1X_1Y_1Z_1$.

3. Novel Control Method

3.1 Kinematics for Included Angle

The idea of the novel control method is to minimize the included angle φ between the moving platform plane and the horizontal plane.

In the fixed coordinate frame $O_1X_1Y_1Z_1$, the plane equation of the horizontal plane $O_1X_1Y_1$ is expressed as:

$$z = 0 \tag{1}$$

If (x, y, z) is the coordinates of any point in the moving platform plane in the fixed coordinate frame $O_1X_1Y_1Z_1$; (x_0, y_0, z_0) is the coordinates of a point in the fixed coordinate system, such as the center C_1 of the moving platform; and A, B, C are the undetermined coefficients. The equation of the moving platform plane in the fixed coordinate frame $O_1X_1Y_1Z_1$ is expressed as:

$$A(x-x_0)+B(y-y_0)+C(z-z_0)=0 \tag{2}$$

The cosine of the included angle φ can be expressed as:

$$\cos\varphi = \frac{|C|}{\sqrt{A^2+B^2+C^2}} \quad (0 \le \varphi \le \frac{\pi}{2}) \tag{3}$$

If (x_i, y_i, z_i) represents the coordinates of the spherical pair b_i in the fixed coordinate frame $O_1X_1Y_1Z_1$ for $i=1,2$ and 3, the coefficients A, B and C can be expressed as:

$$\begin{cases} A=(y_2-y_1)(z_3-z_1)-(z_2-z_1)(y_3-y_1) \\ B=(z_2-z_1)(x_3-x_1)-(x_2-x_1)(z_3-z_1) \\ C=(x_2-x_1)(y_3-y_1)-(y_2-y_1)(x_3-x_1) \end{cases} \tag{4}$$

The coordinate transformation matrix from the coordinate frame $O_2X_2Y_2Z_2$ to the coordinate frame $O_1X_1Y_1Z_1$ can be expressed as:

$$\mathbf{T}=\begin{bmatrix} C\beta C\gamma & -C\beta S\gamma & S\beta & x_T \\ S\alpha S\beta C\gamma + C\alpha S\gamma & -S\alpha S\beta S\gamma + C\alpha C\gamma & -S\alpha C\beta & y_T \\ -C\alpha S\beta C\gamma + S\alpha S\gamma & C\alpha S\beta S\gamma + S\alpha C\gamma & C\alpha C\beta & z_T \\ 0 & 0 & 0 & 1 \end{bmatrix} \tag{5}$$

where $S\alpha$, $S\beta$, $S\gamma$, $C\alpha$, $C\beta$ and $C\gamma$ stand for $\sin\alpha$, $\sin\beta$, $\sin\gamma$, $\cos\alpha$, $\cos\beta$ and $\cos\gamma$ respectively.

The coordinates of the spherical pair b_i in the coordinate frame $O_2X_2Y_2Z_2$ are expressed as:

$$\mathbf{b}_{i,2} = \begin{bmatrix} x_i & y_i & z_i \end{bmatrix}^T_{O_2X_2Y_2Z_2} \tag{6}$$

The coordinates of the spherical pair b_i in the fixed coordinate frame $O_1X_1Y_1Z_1$ are expressed as:

$$\begin{bmatrix} \mathbf{b}_{i,1} \\ 1 \end{bmatrix}_{O_1X_1Y_1Z_1} = \mathbf{T}^{-1} \begin{bmatrix} \mathbf{b}_{i,2} \\ 1 \end{bmatrix}_{O_2X_2Y_2Z_2} \tag{7}$$

Equation (6) can also be expressed as:

$$\begin{cases} \overset{\mathrm{r}}{\mathbf{b}}_{1,2} = \begin{bmatrix} R - l_1 \sin\theta_1 \\ 0 \\ H_1 - l_1 \cos\theta_1 \end{bmatrix} \\ \overset{\mathrm{r}}{\mathbf{b}}_{2,2} == \begin{bmatrix} -\frac{1}{2}R + \frac{1}{2}l_2 \sin\theta_2 \\ \frac{\sqrt{3}}{2}(R - l_2 \sin\theta_2) \\ H_2 - l_2 \cos\theta_2 \end{bmatrix} \\ \overset{\mathrm{r}}{\mathbf{b}}_{3,2} = \begin{bmatrix} -\frac{1}{2}R + \frac{1}{2}l_3 \sin\theta_3 \\ -\frac{\sqrt{3}}{2}(R - l_3 \sin\theta_3) \\ H_3 - l_3 \cos\theta_3 \end{bmatrix} \end{cases} \quad (8)$$

The angles θ_i for $i = 1, 2$ and 3 can be obtained by solving the following equation.

$$\left|\overset{\mathrm{r}}{\mathbf{b}}_{1,2} - \overset{\mathrm{r}}{\mathbf{b}}_{2,2}\right| = \left|\overset{\mathrm{r}}{\mathbf{b}}_{1,2} - \overset{\mathrm{r}}{\mathbf{b}}_{3,2}\right| = \left|\overset{\mathrm{r}}{\mathbf{b}}_{2,2} - \overset{\mathrm{r}}{\mathbf{b}}_{3,2}\right| = \sqrt{3}r \quad (9)$$

3.2 Included Angle Minimization Method

The forward kinematics computational process of the 3-PRS parallel robot is illustrated in Figure 2. The included angle φ between the moving platform plane and the horizontal plane can be calculated based on the feeds of the three prismatic pairs and the relative position and pose between the two coordinate frames. The core of the proposed control method lies in determining the feeds of the three prismatic pairs that minimize the included angle, based on the current relative position and pose as well as the robot's state. The forward kinematics of parallel robots involves nonlinear equations and the issue of multiple solutions, making direct analytical derivation highly challenging. Therefore, nonlinear optimization offers a promising approach for determining suitable feeds of three prismatic pairs.

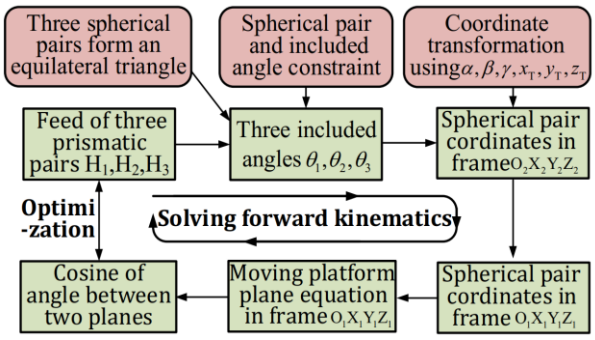

Figure 2: Forward kinematics computational process

4. Implementation Procedure

4.1 Optimization Variable Reduction

The maximum and minimum values of the prismatic pairs are denoted by $H_{\max}$ and $H_{\min}$, respectively. The solution of the novel control method can be transformed into a nonlinear single-objective optimization problem, which can be expressed as:

$$\underset{H_1,H_2,H_3}{\text{minimize}} \ \operatorname{acos}\frac{|C|}{\sqrt{A^2+B^2+C^2}}$$
$$\text{subject to} \begin{cases} H_{\min} \le H_i \le H_{\max} \quad i = 1,2,3 \\ \text{Robot motion continuity} \\ \text{Motion range constraints} \end{cases} \quad (10)$$

From Equation (8), the Z_2-axis coordinates of the three spherical pairs in the frame $O_2X_2Y_2Z_2$ can be expressed as:

$$\begin{cases} z_1 = H_1 - l_1 \cos\theta_1 \\ z_2 = H_2 - l_2 \cos\theta_2 \\ z_3 = H_3 - l_3 \cos\theta_3 \end{cases} \quad (11)$$

If the same value ΔH from both sides is added for each of the equations, Equation (11) can be expressed as:

$$\begin{cases} z'_1 = z_1 + \Delta H = H_1 + \Delta H - l_1 \cos\theta_1 \\ z'_2 = z_2 + \Delta H = H_2 + \Delta H - l_2 \cos\theta_2 \\ z'_3 = z_3 + \Delta H = H_3 + \Delta H - l_3 \cos\theta_3 \end{cases} \quad (12)$$

Substituting z'_1, z'_2, z'_3 for z_1, z_2, z_3, the solution of the Equation (9) remains unchanged. That is to say, according to the property of Equation (9), if the Z_2-coordinate of each spherical pair is increased or decreased by the same value, the solution of Equation (9) remains unchanged. If no special constraint is applied, Equation (8) has an infinite number of solutions. This is because that the objective function in Equation (10) only requires minimizing the included angle between the moving platform plane and the horizontal plane. The pose of the moving platform determines the magnitude of the included angle, whereas its Z_2-coordinate position does not affect it.

Therefore, a new optimization variable reduction strategy is proposed here. During optimization, the feed of one prismatic pair is fixed, and the feeds of the other two prismatic pairs are obtained through optimization. At this point, the height of the moving platform differs from the target height by a certain value. This value should be added to the feeds of all three prismatic pairs simultaneously.

For example, if the feed H_1 is fixed as a constant, Equation (10) is reduced to an optimization problem with two variables, H_2 and H_3. The proposed variable reduction strategy has several advantages. First, reducing the number of optimization variables lowers the complexity of the problem, leading to faster optimization. Second, it addresses the optimization problem with infinite feasible solutions, achieving a strong balance between optimality and feasibility in engineering practice. Finally, by fixing the feed of one prismatic pair to its value at the previous time step, the continuity of robot motion is fully leveraged.

4.2 Selection of Reasonable Solutions

Equation (9) involves trigonometric functions, and due to their periodicity, the equation will yield multiple solutions, including infeasible ones. By applying the kinematic constraints of the joints and motion continuity, unreasonable solutions can be eliminated, only reasonable ones left.

Obtaining direct analytical solutions for nonlinear equations is quite difficult, nor is it particularly necessary; thus, numerical solutions serve as a practical alternative. Derivative-based (gradient-information) iterative methods are employed for solving nonlinear systems of equations. Equation (9) can be written as Equation (13). Since the height of one slider is set as a constant, H_1 is fixed in this study; thus, Equation (13) contains only two unknowns H_2 and H_3, which essentially corresponds to solving for two unknowns with three equations.

$$\begin{cases} \left|\mathbf{b}_{1,2}-\mathbf{b}_{2,2}\right|^2-3r^2=0 \\ \left|\mathbf{b}_{1,2}-\mathbf{b}_{3,2}\right|^2-3r^2=0 \\ \left|\mathbf{b}_{2,2}-\mathbf{b}_{3,2}\right|^2-3r^2=0 \end{cases} \tag{13}$$

Due to the low dimensionality and smooth function, the trust-region dogleg algorithm is used to solve three included angles. Equation (13) may have multiple solutions, while the trust-region dogleg algorithm can only find one solution at a time. Therefore, it is necessary to solve the equations iteratively with multiple different initial values in order to find all the solutions. To enhance both exploration capability and general applicability, adopts a randomized method is adopted to generate initial values for iteration.

In the frame $\mathrm{O_2X_2Y_2Z_2}$ the motion of the spherical pair $\mathrm{b_1}$ and the limb $\mathrm{L_1}$ lies in Plane I; $\mathrm{b_2}$ and $\mathrm{L_2}$ lies in Plane II; and $\mathrm{b_3}$ and $\mathrm{L_3}$ lies in Plane III. Three planes are defined by

$$\begin{cases} y=0 & \text{Plane I} \\ y=-\sqrt{3}x & \text{Plane II} \\ y=\sqrt{3}x & \text{Plane III} \end{cases} \tag{14}$$

Due to constraints such as structural dimensions, the three included angles θ_i for $i=1,2$ and 3 have a certain range of motion. The intersection lines of the three planes can also serve as the limit positions for the motion of the three spherical joints.

4.3 Optimization Procedure

The angle φ is in the interval $[0,\pi/2]$, so to minimize the angle, that is to maximize the cosine of the angle. The objective function is the cosine of the included angle, involving two parameters H_2 and H_3. The objective function TPRS_3HtoCOSPhi comprises the following core functional steps.

Step 1: The three included angles θ_1,θ_2 and θ_3 are computed by solving Equation (13). And unreasonable solutions are eliminated, only reasonable one left. If a feasible solution exists, proceed to Step 3; otherwise, proceed to Step 6.

Step 2: The coordinates of the three spherical pairs b_1,b_2 and b_3 are computed in the frame $\mathrm{O_2X_2Y_2Z_2}$ using the reasonable included angles θ_1,θ_2 and θ_3 through Equation (8).

Step 3: The rotation matrix is computed from $\mathrm{O_2X_2Y_2Z_2}$ to $\mathrm{O_1X_1Y_1Z_1}$ through Equation (5).

Step 4: The coordinates of the three spherical pairs b_1,b_2 and b_3 are computed in the frame $\mathrm{O_1X_1Y_1Z_1}$ through Equation (7).

Step 5: The cosine of the included angle φ is computed through Equation (3). The objective of Equation (10) is to minimize the included angle, which is equivalent to maximizing its cosine value. If it is transformed into a minimization problem for the objective function, then a negative sign needs to be added in front of the objective function.

Step 6: The objective function is assigned a sufficiently small positive value, such as 0.5.

Function TPRS_3HtoCOSPhi computes the negative of the cosine of angle φ based on the feeds of the prismatic pairs of three sliders; however, for certain feed combinations that admit no solution, it will return a sufficiently small positive value, for example 0.5, which carries no geometric meaning as an angle but is solely designated for optimization purposes. Therefore, depending on whether Equation (13) has a feasible solution, the objective function can be reformulated as:

$$f(H_2,H_3)=\begin{cases} -\cos\varphi & \text{with reasonable solution} \\ 0.5 & \text{without reasonable solution} \end{cases} \tag{15}$$

4.4 Implementation Using Genetic Algorithm

This results in the objective function being neither differentiable nor smooth. Therefore, any gradient-dependent optimization algorithm is not applicable. The genetic algorithm possesses a powerful global search capability, does not require gradient information of the objective function, and can effectively handle complex problems such as nonlinear, multi-peak, and combinatorial optimization. They are particularly suitable for solving optimization types that are difficult to address with traditional methods [30]. Therefore, the genetic algorithm is adopted in this study, with the flowchart as shown in Figure 3.

The core performance indicators of genetic algorithms primarily include solution quality, convergence speed, robustness, computational efficiency and success rate. Solution quality refers to the fitness value of the final solution or its gap from the theoretical optimum, while convergence speed refers to the number of iterations or fitness evaluations required to reach a satisfactory solution. In this study, the iteration count and the objective function tolerance are used as the termination criteria for the genetic algorithm. The optimization terminates if either the improvement in the fitness function value over a number of generations is less than the function tolerance, or the iteration count reaches the set limit.

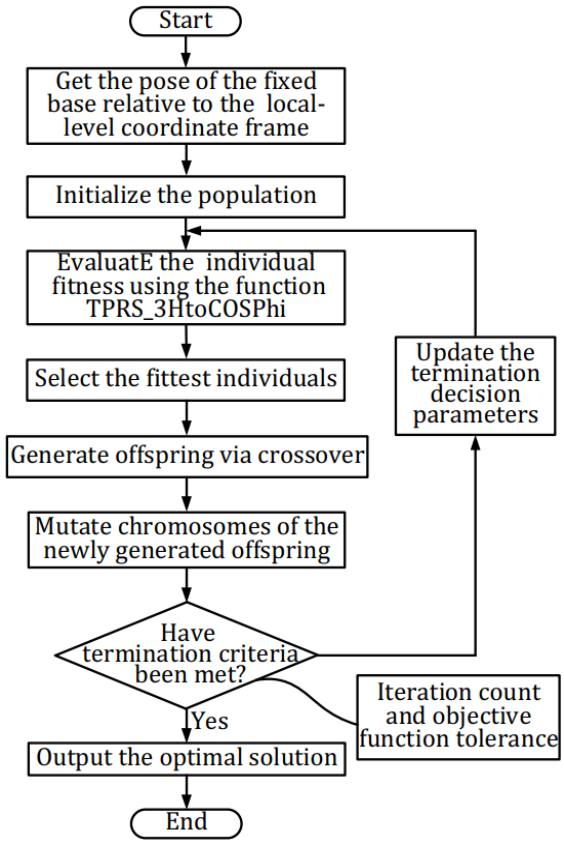

Figure 3: Genetic algorithm optimization flowchart

5. Results and Analysis

5.1 Fundamental Parameters

This section presents several typical cases in order to demonstrate the validity and performance of the novel method proposed in the work. The structural parameters of the 3-PRS parallel robot are as follows: the three limb lengths l_1, l_2 and l_3 are 1100 mm, the fixed base radius R is 500 mm, and the moving platform radius r is 300 mm.

In solving the system of nonlinear equations in Equation (13), the trust-region-dogleg algorithm is adopted and the function tolerance is set as 1e-12. When solving Equation (13), the merging error for distinguishing between the two solutions is set to 1e-10. That is, when the distance between the corresponding components of the two solutions is less than or equal to the merging error, they are considered to be the same solution. In the genetic algorithm, the number of individuals in each generation of the population is set to 100, the maximum number of iterations is set to 200, and the function tolerance is set to 1e-15.

5.2 Cases Where $\beta = \gamma = 0$

The feed H_1 is fixed as a constant value 1700mm. When three Euler angles α, β and γ are $\pi/6$, 0, and 0 respectively, the best score value and mean value versus generation is shown in Figure 4, and the best, worst and mean scores versus generation are shown in Figure 5 in the optimization process.

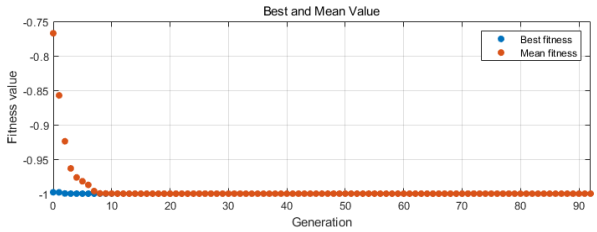

Figure 4: Best and mean value vs. generation

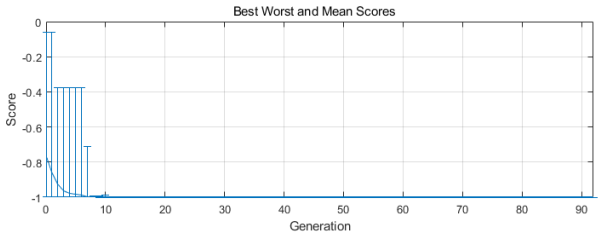

Figure 5: Best, worst and mean scores vs. generation

As can be seen from Figures 4 and 5, the optimization process converges very quickly, with the optimal solution found after just 10 iterations, and every individual in the population has excellent fitness. The optimization yieldes a feasible solution with H_2 at 1818.1710 and H_3 at 1558.3634. At this

point, the cosine of the angle is 1, and the angle is 1.2074e-06 that is a very small number caused by errors and can be considered as 0. That is to say, the moving platform plane is parallel to the horizontal plane through the proposed pose control method.

The optimization results for α at different values are presented in Table 1.

Table 1. Optimization results when $\beta = \gamma = 0$

α , β , γ	H_2 , H_3	$\cos\varphi$	φ
-π/5 ,0 ,0	1530.2026 [H_1-169.7974], 1835.6248 [H_1+135.6284]	1	0
π/5 ,0 ,0	1835.6248 [H_1+135.6284], 1530.2026 [H_1-169.7974]	1	0
-π/6 ,0 ,0	1558.3634 [H_1-141.6366], 1818.1710 [H_1+118.1710]	1	0
π/6 ,0 ,0	1818.1710 [H_1+118.1710], 1558.3634 [H_1-141.6366]	1	0
-π/7 ,0 ,0	1578.7148 [H_1-121.2852], 1804.1674 [H_1+104.1674]	1	0
π/7 ,0 ,0	1804.1675 [H_1+104.1675], 1578.7149 [H_1-121.2851]	1	0
-π/8 ,0 ,0	1594.0542 [H_1-105.9458], 1792.9024 [H_1+92.9024]	1	0
π/8 ,0 ,0	1792.9024 [H_1+92.9024], 1594.0542 [H_1-105.9458]	1	0
-π/9 ,0 ,0	1.6060048 [H_1-93.9952], 1783.7236 [H_1+83.7236]	1	0
π/9 ,0 ,0	1783.7236 [H_1+83.7236], 1606.0048 [H_1-93.9952]	1	0

The following characteristics can be found.

(1) The included angle is 0. That is to say, the moving platform plane is parallel to the horizontal plane. Euler angle α is essentially the rotation angle of the coordinate frame $O_2X_2Y_2Z_2$ about X_1 -axis. Since X_1 -axis is parallel to X_2 -axis, compensation can be achieved by rotating the moving platform in the opposite direction about the moving X_2 -axis by the same angle. Due to the 3-PRS parallel robot being symmetrical about X_2 -axis, optimization can be applied to set the angle to zero.

(2) The optimization results exhibit symmetry. When Euler angle α is equal in absolute value but opposite in sign, the optimized values of H_2 and H_3 are interchanged. Moreover, of the values H_2 and H_3, one is greater than H_1 and the other is less than H_1. The average of the feeds H_2 and H_3 is very close to H_1, but not equal to H_1; rather, it is less than H_1. This phenomenon is caused by the symmetry of the 3-PRS parallel robot. This, to some extent, also demonstrates the validity of the optimization results.

5.3 Cases Where α = γ = 0

The optimization results for β at different values are presented in Table 2. The optimization results show that H_2 and H_3 have the same value. It can be clearly seen from Figure 1 that as the moving platform rotates about the Y_2 -axis, H_2 and H_3 increase or decrease synchronously, which necessarily results in them having the same value.

Table 2. Optimization results when $\alpha = \gamma = 0$

α , β , γ	H_2 , H_3	$\cos\varphi$	φ
0, -π/5 ,0	1454.9770, 1454.9770 [H_1-245.0230]	1	0
0, π/5 ,0	1983.9838, 1983.9838 [H_1+283.9838]	1	0
0, -π/6 ,0	1487.9045, 1487.9045 [H_1-212.0955]	1	0
0, π/6 ,0	1937.9045, 1937.9045 [H_1+237.9045]	1	0
0, -π/7 ,0	1513.9493, 1513.9493 [H_1-186.0507]	1	0
0, π/7 ,0	1904.4447, 1904.4447 [H_1+204.4447]	1	0

5.4 Cases Where α = β = 0

The optimization results for γ at different values are presented in Table 3. Regardless of how the Euler angle γ changes, the optimized values of H_2 and H_3 remain equal to H_1. Since Z_1-axis is parallel to Z_2-axis, the overall rotation of the 3-PRS parallel robot about Z_1-axis does not affect the angle between the moving platform plane and the horizontal plane.

Table 3. Optimization results when $\alpha = \beta = 0$

α, β, γ	H_2, H_3	$\cos\varphi$	φ
0,0, -π/5	H_1, H_1	1	0
0,0, π/5	H_1, H_1	1	0
0,0, -π/6	H_1, H_1	1	0
0,0, π/6	H_1, H_1	1	0
0,0, -π/7	H_1, H_1	1	0
0,0, π/7	H_1, H_1	1	0

5.5 Cases for Different Euler Angles

The optimization results for different Euler angles α, β and γ at different values are presented in Table 4. In all cases where the range of motion of the 3-PRS parallel robot structure permits, the optimization can achieve an angle φ of zero. Meanwhile, the Euler angle γ has no effect on the optimization results.

Table 4. Optimization results for different Euler angles

α, β, γ	H_2, H_3	$\cos\varphi$	φ
π/12, π/12, ±π/12	1878.1003, 1754.9529 [H_1+178.1003, H_1+54.9529]	1	0
π/12, -π/12, ±π/12	1651.9196, 1.515.2593 [H_1-480.8044, H_1-184.7407]	1	0
-π/12, π/12, ±π/12	1754.9529, 1878.1003 [H_1+54.9529, H_1+178.1003]	1	0
-π/12, -π/12, ±π/12	1515.2593, 1651.9196 [H_1-184.7407, H_1-48.0804]	1	0
π/10, π/10, ±π/10	1910.6399, 1767.7415 [H_1+210.6399, H_1+67.7415]	1	0
π/10, -π/10, ±π/10	1642.3373, 1479.8136 [H_1-57.6627, H_1-220.1864]	1	0
-π/10, π/10, ±π/10 +	1767.7415, 1910.6399 [H_1+67.7415, H_1+210.6399]	1	0
-π/10, -π/10, ±π/10	1479.8136, 1642.3373 [H_1-220.1864, H_1-57.6627]	1	0

5.6 Cases with Feed Constraint

In the aforementioned four application cases, optimization achieves parallelism between the two planes; however, when it comes to extreme conditions such as the structural limitations of the 3-PRS parallel robot, the angle φ of zero cannot be attained. Table 5 gives the optimization results for several Euler angles when H_2 and H_3 are constrained in the interval [1500, 1900].

Table 5. Optimization results with feed constraint

α, β, γ	H_2, H_3	$\cos\varphi$	φ
0, -π/5 ,0	1500,1500	0.9902	8.03^0
π/5 , -π/7 ,0	1722.0135, 1500.0000	0.9480	18.55^0
-π/5 , -π/7 ,0	1500.0000, 1722.0135	0.9480	18.55^0
π/5 , -π/6 ,0	1697.4879, 1500.0000	0.9278	21.90^0
π/5 , -π/6 , ±π/7	1.697.4879, 1500.0000	0.9278	21.90^0

From the optimization results, at least one of the optimized values H_2 and H_3 reaches the endpoint of its respective range interval [1500, 1900]. Nevertheless, the method proposed in the study can minimize the angle φ. Of course, when the Euler angles are too large, constraints such as the motion ranges of the 3-PRS parallel robot's components-including its spherical joints and revolute joints-prevent the angle from being minimized to zero. The 3-PRS parallel robot has two rotational degrees of freedom. When the structure allows, these two degrees can be used to compensate for the orientation of the fixed base, keeping the moving platform parallel to the horizontal plane. When the

structure does not allow it, complete compensation is not possible, and the angle can only be minimized.

5.7 Cases for Multi-stage Optimization

The discussion in Section 5.6 also provides a new idea for determining the variable interval adjustment for genetic algorithm optimization. A multi-stage approach can be used for optimization. Specifically, the optimization variables can first be confined to a relatively small range for improving optimization efficiency. When the feasible solution reaches the endpoint of the interval, the range is expanded in the direction of that endpoint and optimization is performed again. These stages can be repeated multiple times until the optimal solution is obtained. Two instances are shown in Table 6, both of which obtain the optimal solution after two stages of optimization.

Table 6. Cases Results for Multi-stage optimization

Item	α , β	π/9 , π/9	-π/9 , -π/9
First stage	Range interval	[1500, 1900]	[1500,1900]
	H_2 , H_3	1900.0000, 1753.5917	1500.0000, 1652.7231
	$\cos\varphi$	0.9976	0.9961
	φ	3.94^0	5.09^0
Second stage	Range interval	[1700,2000]	[1400,1800]
	H_2 , H_3	1931.5368, 1776.7166	1456.7176, 1635.8996
	$\cos\varphi$	1	1
	φ	0	0

6. Conclusions

This study proposes a novel pose control method for the 3-PRS parallel robot moving platform, which fully takes into account the variation in the pose of the fixed base.

(1) The structure and equivalent model of the 3-PRS parallel robot is presented. The coordinate systems of the robot and the local-level horizontal plane are established.

(2) A novel real-time pose control method for the moving platform is proposed. The new method takes the angle between the horizontal plane and the moving platform plane as the core metric. The detailed expression of the angle and its derivation process are both presented.

(3) An implementation method is proposed for the proposed control method. The new control method is transformed into a constrained nonlinear optimization problem. A novel strategy is proposed to transform the optimization problem with three variables into one with two variables.

(4) The genetic algorithm is proposed to solve the optimization problem in this study, and the calculation process is given. The study proposes that the interval range of the optimization variables is adjusted using a multi-stage method to find the global optimal solution while maintaining efficiency.

The proposed method is validated in terms of its effectiveness, practicality, and feasibility. The results show that the proposed method has many advantages and beneficial effects as follows.

(1) The proposed method uses the parallelism between the moving platform plane and the horizontal plane as the evaluation metric, which is transformed into the objective of minimizing the angle between the two planes. This minimizes the impact of changes in the fixed base pose on the 3-PRS parallel robot, thereby ensuring operational stability.

(2) In the given typical application cases, through optimization, the angle between the moving platform plane and the horizontal plane is always minimized, i.e., they are parallel to each other. Even when structural constraints of the 3-PRS parallel robot prevent the two planes from being parallel, the angle between them can still be minimized.

(3) The proposed method effectively addresses issues such as multiple solutions and nonlinearity in the 3-PRS parallel robot, enabling the solution process to proceed smoothly.

(4) The employment of numerical calculation methods avoids the issues of multiple branches and complex judgment that are often encountered in analytical methods for the forward kinematics analysis of 3-PRS parallel robots.

It should be noted that this study is focused on the application of vehicle-mounted drone hangars; for applications in other fields, the motion platform is not necessarily required to be parallel to the horizontal plane. Even if there are specific requirements for the orientation of the motion platform relative to the horizontal plane, the method proposed in this study remains highly applicable, simply by replacing the optimization objective with the required orientation.

In summary, the study provides a theoretical basis and timely support for the high-precision pose control of equipment on mobile platform, such as those used in intelligent production line, emergency rescue vehicle and intelligent driving.

Acknowledgement

This research was funded by the Science and Technology Key Project of Henan Province, China (Grant No. 262102241006). The authors would also like to thank the anonymous reviewers for their insightful comments and constructive suggestions, which greatly improved the quality of this paper.

References

[1] Huang, J., Huangfu, C., Zhang, J., Cai, J., Li S. Liu, Z., Yan, Y., Chen, G.(2025) Dynamic Decoupling and Control of 3-PRS Parallel Mechanism. Transactions of the Chinese Society for Agricultural Machinery, 56(6), 0735-744. https://doi.org/10.6041/j.issn.1000-1298.2025.06.069

[2] Chen, G., Fan, Q., Luo, C.(2022) Comparison of attitude capability of 3-PRS parallel mechanism with different chain arrangement. Manufacturing Technology & Machine Tool, 2022(10), 54-60. https://doi.org/10.19287/j.mtmt.1005-2402.2022.10.007

[3] Zheng, Y., Liu, J., Lin, C., Guang C., Yang Y., Yu, J., Ma, K., Xu, F. (2025) Dynamic modeling, optimization, and validation of a handheld 3-PRS compliant robot with coupled bending-torsion deformation. Nonlinear Dynamics, 113(25), 34707-34731, https://doi.org/10.1007/s11071-025-11837-2

[4] Zhang, H., Yang, J., Gao, S., Gong, X., Zhu, W.(2025) Feedrate scheduling method for 3-PRS hybrid machine tools considering kinematic constraints. Robotics and Computer-Integrated Manufacturing, 95, Article number:102988, https://doi.org/10.1016/j.rcim.2025.102988

[5] Zhao, F., Xu, D., Jin, X., Ding, X., Guo, S., Xu, K., Fang, Y.(2024) In-hand manipulation using a 3-PRS-finger-based parallel dexterous hand with bidirectional pinching capability. Mechanism and Machine Theory, 192, Article number:105553, https://doi.org/ 10.1016/j.mechmachtheory.2023.105553

[6] Zermane, A., Guiatni, M., Alouane, M., Alloun, F., Tair, M.(2023) Optimal mechatronics design and control of a 3-PRS robotic platform for vertigo diagnosis, 2023 International Conference on Control, Automation and Diagnosis, ICCAD 2023, https://doi.org/10.1109/ICCAD57653.2023.10152397

[7] Chen, G., Zhou, H., Huang, J., Liu, M., Bai, B.(2022) Position and pose measurement of 3-PRS ankle rehabilitation robot based on deep learning. Recent Advances in Computer Science and Communications, 15(2), 284-297, https://doi.org/10.2174/2666255813999200831102550

[8] Wang, J. Liang, H., Guan, D., Wang, X., Shen, H. (2012) 3-PRS parallel robot for battery swapping of electric vehicle. 2012 IEEE International Conference on Mechatronics and Automation, ICMA 2012, Article number: 6285752, https://doi.org/10.1109/ICMA.2012.6285752

[9] Dai, L., Xu, Q., Chen, X., Zeng, D., Guo, R., Cai, C.(2022)A 3-PRS parallel numerical control machine tool swing angle deviation detection and compensation method. Journal of Physics: Conference Series, 2378(1), Article number: 012046, https://doi.org/10.1088/1742-6596/2378/1/012046

[10] Liu, Y., Wu, J., Wang L., Zhao, J., Wang, J., Yu, G..(2017) A novel symmetrical 3-DOF PKM and its performance comparison with 3-PRS PKM. High Technology Letters, 23(2), 131-140, https://doi.org/10.3772/j.issn.1006-6748.2017.02.003

[11] Quan, H., Lin, G., Huang, J., Liang, J., Wang, T., Liao, X.(2022). Kinematic analysis of 3-PRS & 3P hybrid mechanism. Machine Tool & Hydraulics, 50 (4), 36-40. https://doi.org/10.3969/ j.issn.1001-3881.2022.04.007

[12] Chen, G., Zhou, H., Huang, J., Dai, J., Bai, B., Liu, M.(2021) Dynamic modeling with joint friction of 3-PRS parallel mechanism. Transactions of the Chinese Society for Agricultural Machinery, 52(8), 416-426. https://doi.org/10. 6041/j.issn.1000-1298.2021.08.043

[13] Hu, B., Shi, D., Shi, Y., Zhang, D., Ye, N.(2020). Kinematically identical manipulators for an asymmetric 3-PRS parallel manipulator and their constraint performance comparison study. Journal of Mechanical Engineering. 56(3),31-40, https://doi.org/10.3901/JME.2020.03.031

[14] Wei, J., Bi, H. Yao, H., Chen, F.(2023). An inverse kinematic model for the 3-PRS compliant parallel mechanism with forward causative force. IEEE Access, 11, 135283-135294, https://doi.org/10.1109/ACCESS.2023.3337835

[15] Chen, G. Zhou, H., Yang, P. (2020) Force/position control strategy of 3-PRS ankle rehabilitation robot. International Journal of Innovative Computing, Information and Control, 16(2), p 481-494, https://doi.org/10.24507/ijicic.16.02.481

[16] Tavoosi, J., Mohammadi, F.(2019) A 3-PRS parallel robot control based on fuzzy-PID controller. 6th International Conference on Control, Instrumentation and Automation, ICCIA 2019,Article number:9030860, https://doi.org/10.1109/ICCIA49288.2019.9030860

[17] Yuan, H., Liu, Z., Huang, S.(2025) Optimization analysis of 3-PRS parallel robot control. Journal of Physics: Conference Series, 3060(1), Article number: 012044. https://doi.org/10.1088/1742-6596/3060/1/012044

[18] Chen, G., Zhou, H., Huang, J., Guo, D., Kang, J., Kang, J. Driving force estimation of 3-PRS parallel robot based on deep learning. International Journal of Mechatronics and Applied Mechanics, 2024(15), 79-89,https://doi.org/10.17683/ijomam/issue15.10

[19] Tossaporn, U., Sakda, C.; Siwat, L.; Teeranoot, C. Kinematics of platform stabilization using a 3-PRS parallel manipulator. ROBOMECH Journal, 10(1), Article number:8, https://doi.org/10.1186/ s40648-023-00247-x

[20] Ma, Y.W., Tian, Y.L.,Liu, X.P., Lu, C.H.(2023)Dynamic modeling and analysis of the 3-PRS power head based on the screw theory and rigid multipoint constraints. Science China Technological Sciences, 66(7),1869-1882, https://doi.org/10.1007/s11431-022-2369-0

[21] Sun, F. W., Yuan, Z. T., Chen, G. Q.(2023) Kinematics analysis and driving stroke optimization of 3-PRS compliant parallel mechanism. Journal of Henan Polytechnic University (Natural Science), 42(2),87-97. https: //doi.org/10.16186/j.cnki.1673-9787.2021060093

[22] Huang, S. Zhu., W., Yang, J., Chen, Y.(2019). Kinematics analysis of 3-PRS+2P hybrid mechanism, 43(3), 104-108, https://doi.org/ 10.16578/j.issn.1004.2539.2019.03.019

[23] Nigatu, H., Li, J., Zhu, K.; Zhang, J.; Guo., H.; Lu, G., Kim, D.(2024) The stiffness of 3-PRS PM across parasitic and orientational workspace. Proceedings of 6th International Conference on Reconfigurable Mechanisms and Robots, ReMAR 2024, p 159-164, 2024, https://doi.org/ 10.1109/ReMAR61031.2024.10617674

[24] Pundru, Srinivasa Rao(2022) Synthesis of Multi-position 3-PRS manipulator based on spherical constraints by eliminating the parasitic motion. Journal of The Institution of Engineers(India):Series C, 103(6),1447-1454, https://doi.org/10.1007/s40032-022-00887-9

[25] Ma, Y., Tian, Y., Song, Y.(2022) A screw theory-based approach for conservative stiffness mapping of 3-PRS parallel mechanism. Proceedings of the 4th WRC Symposium on Advanced Robotics and Automation 2022, https://doi.org/10.1109/WRCSARA57040.2022. 9903927

[26] Nigatu, H., Choi, Y. H., Kim, D.(2021) Analysis of parasitic motion with the constraint embedded Jacobian for a 3-PRS parallel manipulator. Mechanism and Machine Theory, 164,Article number:104409, https://doi.org/ 10.1016/j.mechmachtheory.2021.104409

[27] Vallés, M., Cazalilla, J., Valera, Á. Mata, V., Page, Á., DIáz-Rodríguez, M.(2017) A 3-PRS parallel manipulator for ankle rehabilitation: Towards a low-cost robotic rehabilitation.Robotica,35(10), 1939-1957, https://doi.org/10.1017/S0263574715000120

[28] Ruiz, A., Campa, F.J., Roldán-Paraponiaris, C., Altuzarra, O., Pinto, C. (2016) Experimental validation of the kinematic design of 3-PRS compliant parallel mechanisms, Mechatronics, 39, 77-88, https://doi.org/10.1016/j. mechatronics. 2016.08.006

[29] Zhang, J., Wu, J. (2026) Dimensional synthesis of a 3-PRS parallel manipulator for UAV-based wind turbine inspection: a task-oriented multi-objective optimization approach. Proceedings of the International Conference on Automation, Robotics and Applications, ICARA 2026, https://doi.org/10.1109/ICARA69401.2026.114 80309

[30] Li, Y., Yu, B., Li, X., Luo, S., Li, H. (2020) Application and realization of genetic algorithm based on MATLAB environment. Advances in Intelligent Systems and Computing, 928,979-985, https://doi.org/10.1007/978-3-030-15235-2_ 130